Heliyon 10 (2024) e34490

Contents lists available at ScienceDirect

Heliyon

journal homepage: www.cell.com/heliyon

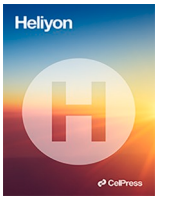

Research article

O-GlcNAc modification in endothelial cells modulates adiposity via fat absorption from the intestine in mice

Seiichiro Ohgaku [a], Shogo Ida [a,*], Natsuko Ohashi [a,b,**], Katsutaro Morino [a,c], Atsushi Ishikado [a,d], Tsuyoshi Yanagimachi [a], Koichiro Murata [a], Daisuke Sato [a], Satoshi Ugi [a], Ali Nasiri [e], Gerald I. Shulman [e,f], Hiroshi Maegawa [a], Shinji Kume [a], Yukihiro Fujita [a,***]

[a] *Department of Medicine, Shiga University of Medical Science, Otsu 520-2192, Japan*
[b] *Department of Stem Cell Biology and Regenerative Medicine, Shiga University of Medical Science, Otsu 520-2192, Japan*
[c] *Institutional Research Office, Shiga University of Medical Science, Otsu 520-2192, Japan*
[d] *R&D Department, Sunstar Inc., Osaka 569-1195, Japan*
[e] *Department of Medicine (Endocrinology), Yale School of Medicine, New Haven, CT 06520, USA*
[f] *Department of Cellular & Molecular Physiology, Yale School of Medicine, New Haven, CT 06520, USA*

ARTICLE INFO

Keywords:
Obesity
Endothelial cell
O-GlcNAcylation
Lipid absorption
Vascular endothelial growth factor receptor 3
Nitric oxide

ABSTRACT

Introduction: Endothelial cells have a crucial function in transporting and exchanging various nutrients. *O*-GlcNAcylation, mediated by *O*-GlcNAc transferase (OGT), involves the addition of *N*-acetylglucosamine to proteins and serves as an intracellular nutrient sensing mechanism. However, the role of *O*-GlcNAcylation in endothelial cells remains poorly understood.
Objective: This study investigated the role of *O*-GlcNAcylation in endothelial cells.
Methods: Endothelial-cell-specific *Ogt* -knockout mice (*Ogt*-ECKO) were generated by crossing *Ogt*-floxed mice (*Ogt*-flox) with *VE-Cadherin* Cre ER^{T2} mice. *Ogt*-ECKO mice and *Ogt*-flox control mice were subjected to a normal or high-fat diet, and their body weight, glucose metabolism, and lipid metabolism were examined.
Results: *Ogt*-ECKO mice exhibited reduced body weight compared with *Ogt*-flox control mice under a high-fat diet. Lipid absorption was significantly impaired in *Ogt*-ECKO mice. Changes in the intercellular junctions of small intestinal lacteal endothelial cells from a button-like to a zipper-like configuration were observed. Furthermore, *Ogt*-ECKO mice showed decreased expression of VEGFR3. The administration of a nitric oxide donor restored lipid absorption and reversed the morphological alterations in *Ogt*-ECKO mice.
Conclusions: These findings demonstrate the critical role of *O*-GlcNAcylation in endothelial cells in lipid absorption in the intestine through the modulation of lacteal junction morphology. These results provide novel insight into the metabolic regulatory mechanisms under physiological conditions and have implications for the development of new therapeutic strategies for obesity.

* Corresponding author.
** Corresponding author. Department of Medicine, Shiga University of Medical Science, Otsu, 520-2192, Japan.
*** Corresponding author.
E-mail addresses: idashogo@belle.shiga-med.ac.jp (S. Ida), natsu514@belle.shiga-med.ac.jp (N. Ohashi), fujita@belle.shiga-med.ac.jp (Y. Fujita).

https://doi.org/10.1016/j.heliyon.2024.e34490
Received 8 October 2023; Received in revised form 10 July 2024; Accepted 10 July 2024
Available online 14 July 2024

1. Introduction

The vascular system can be divided into two major types: the blood vessel system and the lymphatic system. These systems are distributed throughout the body and form a network. The blood vessel system carries blood, while the lymphatic system carries lymph fluid. The blood system, centered around the heart, carries nutrients and paracrine signaling molecules, transports cells and metabolites, and facilitates gas exchange throughout the body [1]. In contrast, the lymphatic system is a network with blind ends [2]. It collects interstitial fluids, including metabolic waste, and channels them into venules. Although the two systems function separately, both blood and lymph vessels are identically composed of endothelial cells (ECs) and consist of a single layer of ECs.

Abbreviations

IPGTT	Intraperitoneal glucose tolerance test
IPITT	Intraperitoneal insulin tolerance test
IVLTT	Intravenous lipid tolerance test
NO	Nitric oxide
O-GlcNAcylation	*O*-linked *N*-acetylglucosaminylation
OGA	*O*-GlcNAcase
OGT	*O*-GlcNAc transferase
OGTT	Oral glucose tolerance test
OLTT	Oral lipid tolerance test
VEGF	Vascular endothelial growth factor
VEGFR	Vascular endothelial growth factor receptor

Vascular endothelial growth factor (VEGF) and vascular endothelial growth factor receptor (VEGFR) signaling regulate permeability through the phosphorylation of VE-Cadherin [3]. Recent studies have highlighted the crucial role of VE-Cadherin in lymphatic vessel formation and the regulation of permeability [4,5]. In addition, VEGF influence the movement of nutrients within tissues by affecting the junctions between endothelial cells and altering permeability. Excessive consumption of dietary lipids is a major contributing factor to the development of obesity. The absorption of lipids takes place through the lymphatics found in the intestinal villi, and the proper functioning of lymphatic endothelial cells (LECs) is essential for this process. Studies have revealed that a decrease in CD36 expression within LECs can disrupt the integrity of the lymphatic system and impair lipid absorption. Furthermore, changes in VEGF signaling have been implicated in these alterations [6]. Previous reports have shown that changes in VEGF signaling can convert lymphatic endothelial cell-cell junctions from discontinuous button-like junctions (button junction) to continuous zipper-like junctions (zipper junction) [7], and conversion of junctions from buttons to zipper has been associated with decreased lipid absorption from the intestines. Consequently, LECs play a significant role in the development of obesity, and their metabolic regulation is influenced by VEGF signaling.

Recently, the hexosamine biosynthetic pathway (HBP), which is a collateral pathway of glycolysis, has garnered significant attention in the field of glucose metabolism research. This pathway involves the conversion of fructose-6-phosphate into uridine diphosphate *N*-acetylglucosamine (UDP-GlcNAc). The HBP pathway is noteworthy because it integrates amino acids and fatty acids into its synthesis, making it a nutrient sensor within cells [8–10]. UDP-GlcNAc, the final product of the HBP, serves as the donor substrate for O-linked *N*-acetylglucosamine (*O*-GlcNAc) modification [11]. *O*-GlcNAcylation occurs on serine/threonine residues of proteins and takes place in the nucleus, cytoplasm, and mitochondria [12]. This modification is regulated by two enzymes: *O*-GlcNAc transferase (OGT), which facilitates *O*-GlcNAc modification, and *O*-GlcNAcase (OGA), which reduces it [13].

It has been reported that OGT is strongly associated with the regulation of body weight. Indeed, we observed that mice with whole-body deficiency of OGT induced by tamoxifen showed significant weight loss, leading to increased mortality [14]. Additionally, we and other group found that the loss of *O*-GlcNAcylation specifically in intestinal epithelial cells was associated with body weight loss through the malabsorption of glucose [15,16]. Besides, there are various reports on the effect of *O*-GlcNAcylation on body weight. For instance, the enhancement of *O*-GlcNAcylation in adipose tissue promotes diet-induced obesity [17], in contrast, the high-fat diet fed adipose tissue-specific *Ogt* knockout mice suppressed body weight gain due to inhibition of the healthy expansion of adipose tissue [18]. Neuronal *O*-GlcNAc transferase activation was shown to regulate appetite [19]. Hepatic *O*-GlcNAcylation aberrations lead to elevated blood glucose levels by inhibiting insulin signaling, stimulating gluconeogenesis, and inhibiting glycogen synthesis [20]. These reports suggest that *O*-GlcNAcylation may regulate body weight and glucose metabolism through tissue-specific functions, potentially acting as a nutritional sensor. However, the precise role of *O*-GlcNAcylation in endothelial cells, particularly its relationship with body weight regulation and nutrient absorption, remains unclear.

To address this knowledge gap, our study aimed to investigate the role of *O*-GlcNAcylation in endothelial cells. For this purpose, we generated mice with endothelial-cell-specific deficiency of *Ogt* (*Ogt*-ECKO). In addition, we evaluated their VEGFR expression and the involvement of nitric oxide (NO).

2. Material and methods

2.1. Animal experiment

Ogt-KO mice were generated using the Cre-LoxP system. We crossbred *Ogt*-flox female mice (The Jackson Laboratory, Bar Harbor, ME, USA) with *VE-Cadherin-Cre-ER*^{T2} male mice (donated by Dr. Yoshiaki Kubota) to generate *Ogt*-ECKO mice. All experiments and analyses were performed using male mice, as females are protected from diet-induced insulin resistance. Age-matched *Ogt*-flox male mice were used as controls. Mice were group-housed in a light- and temperature-controlled facility, with lights on from 8 a.m. to 8 p.m. and a temperature of 25 °C. Tamoxifen (T5648; Sigma-Aldrich, St. Louis, MO, USA) was intraperitoneally injected for 5 consecutive days at a dosage of 0.15 g/kg/day when the mice were 8–10 weeks of age (normal diet: ND). For genotyping, DNA was extracted from the tails of the mice, and PCR was performed using primers for *Ogt*-flox and *Cre* (primer sequences are listed in the Supplemental Table). The PCR for *Ogt*-flox was conducted following the protocol provided by the mouse distributor, Jackson Laboratory (https://www.jax.org/Protocol?stockNumber=004860&protocolID=22622). The PCR for *Cre* was performed according to a previously reported method (Fig. S1) [21]. The reduction of *O*-GlcNAcylation in vascular endothelial cells and lymphatic endothelial cells after tamoxifen administration was confirmed using Western blotting and immunofluorescent staining (Figs. 1B and 5B). For high-fat-diet (HFD) feeding experiments, the mice were fed an HFD (60 kcal%; Research Diets Inc., New Brunswick, NJ, USA) 1 week after

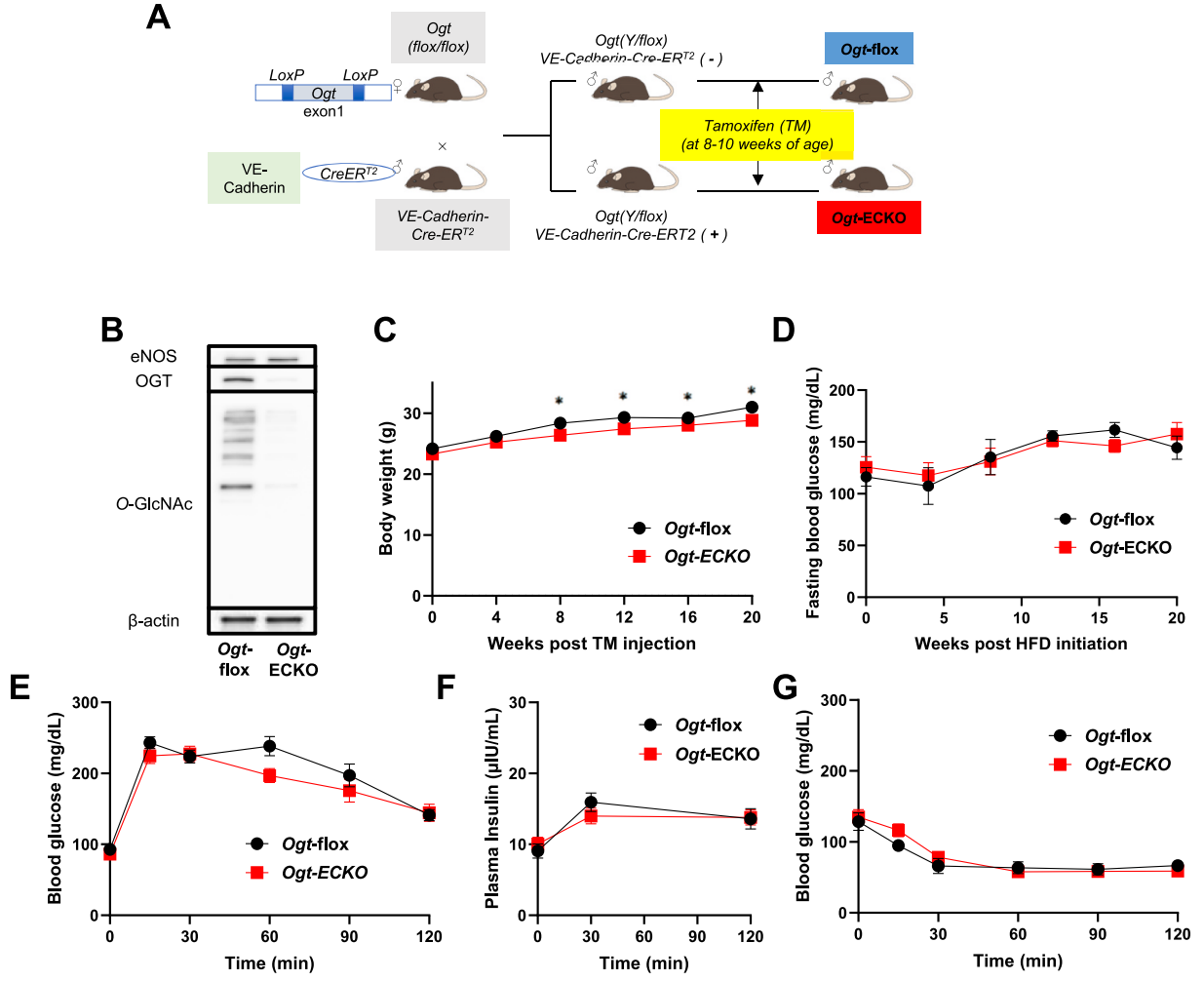

Fig. 1. Under a normal diet, *Ogt*-ECKO mice had slightly reduced weight gain compared with *Ogt*-flox mice, but there was no significant impact on glucose metabolism.
A: Schematic diagram of *Ogt*-ECKO mouse generation. B: Representative Western blot analysis of OGT and *O*-GlcNAcylation (RL2) in the primary-cultured endothelial cells at 8 weeks after TM injection. C, D: Body weight (C) and fasting blood glucose (D) changes in *Ogt*-flox and *Ogt*-ECKO mice (n = 5–6). E–G: Changes in blood glucose levels during IPGTT (E) and IPITT (G), and plasma insulin levels during IPGTT (F) at 8 weeks after tamoxifen injection (n = 7–12).
Data are presented as the mean ± SEM. *p < 0.05, ns: not statistically significant.

tamoxifen injection. All animal handling and experimentation were conducted in accordance with the Research Center for Animal Life Science guidelines at Shiga University of Medical Science (approval numbers 28–32, 31–45, and 3–14) or Yale University. All experimental protocols were approved by the Gene Recombination Experiment Safety Committee and Research Center for Animal Life Science at Shiga University of Medical Science or Yale University Institutional Animal Care and Use Committee.

2.2. Tissue collection

Mice that were fed an HFD for either 4 weeks or 24 weeks were used. Prior to tissue collection, the mice were euthanized by the intraperitoneal administration of 10 % pentobarbital with sevoflurane inhalation at different time points. Inguinal white adipose tissue (iWAT), epididymal white adipose tissue (eWAT), interscapular brown adipose tissue (BAT), liver, intestine, and lung were dissected immediately and stored for subsequent analysis.

2.3. Histological analyses

For histological analyses, samples embedded in paraffin were sectioned at 3 mm thickness. To determine adipocyte counts, three randomly selected views from five animals of both *Ogt*-flox and *Ogt*-ECKO mice were analyzed. Transmission electron microscopic analysis of the intestine was performed with a Hitachi H-7500 (Hitachi, Tokyo, Japan). For whole-mount staining, transcardial perfusion was conducted with 4 % paraformaldehyde (PFA) after anesthesia. The jejunum was then removed and longitudinally cut to expose the lumen. After several washes with phosphate-buffered saline (PBS), the samples were post-fixed in 4 % PFA for 2 h at 4 °C. Subsequently, the samples were washed several times with PBS and dehydrated in 10 % sucrose in PBS for 2 h, followed by 20 % sucrose and 10 % glycerol in PBS overnight. The samples were washed multiple times with PBS before blocking. Blocking was performed using 5 % goat serum in 0.5 % Triton-X 100 in PBS (PBST) for 1 h. Next, the samples were incubated overnight at 4 °C with primary antibodies against lymphatic vessel endothelial hyaluronan receptor 1 (LYVE-1; a homolog of the hyaluronan receptor CD 44) (11–034; Angiobio, San Diego, CA, USA) and VE-Cadherin (550548; BD Biosciences, San Jose, CA, USA) diluted in the blocking solution. After several washes with PBST, the samples were incubated with the indicated fluorochrome-conjugated secondary antibodies, diluted in blocking buffer, for 2 h at room temperature (RT). Following a final wash with PBS, the samples were mounted with Vectashield (Vector Laboratories). Images were captured using a TCS SP8 confocal microscope (Leica Microsystems). The areas of LYVE-1 positive and VE-cadherin positive regions were quantified using ImageJ, following the methodology outlined in previous literature [22].

2.4. Hematological and fecal analyses

Blood glucose concentrations were measured with glucose dehydrogenase–pyrroloquinoline quinone glucose test strips (Glutest Sensor or Glutest Neo Alfa; Sanwa Kagaku Kenkyusho, Nagoya, Japan). Plasma insulin levels were measured by ELISA (M1104; Morinaga, Kanagawa, Japan). Fecal TG extraction was performed using the Bligh and Dyer protocol [23]. Serum and fecal triglyceride (TG) levels were measured by LabAssay™ Triglyceride (632–50991; Fujifilm Wako, Osaka, Japan). Serum free fatty acid (FFA) levels were measured using LabAssay™ NEFA (632–52001; Fujifilm Wako). Serum NO concentrations were measured using Nitrate/Nitrite Colorimetric Assay Kit (780001; Cayman Chemical, Michigan, USA).

2.5. Intraperitoneal and oral glucose tolerance tests

An intraperitoneal glucose tolerance test (IPGTT) and oral glucose tolerance test (OGTT) were performed on *Ogt*-ECKO and control mice after an overnight fast. The mice were either intraperitoneally injected or orally administered glucose at a dosage of 1 g/kg. Blood glucose levels were measured 0, 15, 30, 60, 90, and 120 min later, while plasma insulin levels were measured 0, 30, and 120 min later.

2.6. Intraperitoneal insulin tolerance test

Ogt-ECKO and *Ogt*-flox mice were intraperitoneally injected with insulin (0.5 units/kg) after a 6-h fast. Blood glucose levels were determined 0, 15, 30, 60, 90, and 120 min later.

2.7. Oral lipid tolerance test

For the oral lipid tolerance test (OLTT), *Ogt*-ECKO and control mice were orally administered 0.5 mL of olive oil after an 18-h fast. Blood collection was performed before administration and 1, 2, 3, 4, 6, and 8 h after it. Serum TG and FFA levels were measured. The analysis of TG fractions before and after OLTT using HPLC was performed by LipoSEARCH (Immuno-Biological Laboratories) (Gumma, Japan). Tyloxapol was used in experiments to exclude the influence of lipoprotein lipase (LPL). 500 mg/g Tyloxapol (Triton WR1339; T0307; Sigma-Aldrich) was injected before oral lipid loading and serum samples were collected.

2.8. Intravenous lipid tolerance test

An intravenous lipid tolerance test was performed as described previously [24]. Briefly, Intralipos® 20 % (Otsuka Pharmaceutical,

Tokyo, Japan) was injected into the tail vein with or without 500 mg/g Tyloxapol after an 18-h fast. Blood collection was performed 1, 3, 6, 10, and 15 min later, with the collected samples used to measure serum TG and FFA levels.

2.9. Hepatic very low-density lipoprotein (VLDL)-TG secretion tests

Hepatic VLDL-TG production was determined as described previously [25]. Mice were intravenously injected with 20 mg of tyloxapol in 100 mL of PBS. Serum samples were collected before the injection of tyloxapol and at 30-min intervals after it for up to 2 h, which were used to measure TG in VLDL.

2.10. Oral lipid tolerance test with NO donor

In accordance with a previous report [26], *Ogt*-flox and *Ogt*-ECKO mice were subcutaneously injected with NO donor (DETA--NONOate; 82120; Cayman Chemical, Ann Arbor, MI, USA) at a dose of 1.0 μg/g body weight (BW) for 10 consecutive days, starting 1 week after the initiation of HFD. A vehicle-treated control group was also included. In each group, changes in body weight between before and after NO donor administration were measured. OLTT was performed at the end of the NO donor administration period and serum TG levels were measured.

2.11. Body composition and basal metabolism analysis

Body weight was monitored monthly using a digital precision scale with an accuracy of 0.1 g. Body composition, including fat and lean mass, was assayed using an EchoMRI system. Mice were individually housed for at least 1 week before the energy intake analysis to allow for environmental habituation. Energy intake was calculated by multiplying the consumed food quantity by the energy density of 5.24 kcal/g. Food consumption was manually weighed using a digital precision scale with an accuracy of 0.01 g.

For basal metabolism measurement, the mice were acclimated in metabolic chambers (Promethion Systems; Sable Systems International, North Las Vegas, NV, USA) for 5 days. Gas exchange and ambulatory activity were continuously recorded for another 2 days. The ambulatory activity was detected using beam motion detectors positioned around the cage, which counted the number of beam breaks.

2.12. Primary cultured vascular endothelial cells

To evaluate protein expression and *O*-GlcNAcylation in vascular endothelial cells, primary-cultured vascular endothelial cells were used. Mice that had been fed an HFD for 4–8 weeks were euthanized following the previously mentioned procedure. All lung lobes were excised, and the lungs were minced into approximately 3-mm pieces. Collagenase A (10,103,586,001; Roche, Tokyo, Japan) was added to the minced lung, followed by 1-h incubation. The lung cells were then passed through a 40-μm cell strainer and centrifuged at 1000 rpm for 5 min. Next, the cells were resuspended in Endothelial Cell Growth Medium (ECGM) (C-22110; Promocell, Heidelberg, Germany), transferred into a collagen-coated 10-cm dish, and incubated at 37 °C in a cell incubator with 5 % CO_2. When the cell culture reached sub-confluence, the cells were collected and placed in a 15-mL Corning tube. The tube was supplemented with a mixture of 20 μL of ICAM-2 antibody (553326; BD Biosciences) and 50 μL of Dynabeads conjugated with sheep anti-rat IgG (DB10007; Thermo Fisher, Waltham, MA, USA) in 10 mL of PBS/0.2 % bovine serum albumin (BSA) and incubated for 30 min at 4 °C. Then, the tube was placed on a magnet for 1 min. After removing the supernatant, the tube was taken off the magnet, 10 mL of PBS/0.2 % BSA was added, and the tube was placed on the magnet again for 1 min. The supernatant was removed once more, the tube was taken off the magnet, 10 mL of ECGM was added, and the contents were spread in a 10-cm dish. When the cell culture reached confluence, the cells were collected for western blotting.

2.13. Isolation of intestinal lymphatic endothelial cells by flow cytometry

In accordance with a previous report [27], transcardial perfusion with PBS was performed after anesthesia and the small intestine was removed. The serosa, muscular layer, mesenteric fat, and Peyer's patches were then dissected from the small intestine. After the intestinal fragments had been opened longitudinally and washed with PBS, the samples were cut into 2-cm pieces. These samples were incubated with 10 mM EDTA in calcium- and magnesium-free DMEM (Gibco) for 20 min on ice. Subsequently, the tissues were vortexed with PBS, further cut into 1-mm fragments, and dissociated with dissociation buffer containing 2 mg/mL collagenase A (Roche), 1 mg/mL Dispase (Gibco), and 1 U/mL DNase (Invitrogen) in DMEM at 37 °C for 30 min. The resulting mixture was filtered through a 70-μm strainer and the supernatants were collected. An equal volume of DMEM was added to the collected supernatants. After centrifugation, the cells were resuspended in PBS, suspended in Flow Cytometry Staining Buffer (eBiosciences, Inc., San Diego, CA, USA), and stained with a Biotin Mouse Lineage Panel, which includes the LYVE-1 antibody (MAB2125; R&D), followed by fluorescent antibodies: phycoerythrin (PE)-Cy7-conjugated streptavidin, allophycocyanin (APC)-conjugated anti-*c*-kit, and APC-Cy7-conjugated anti-Ly6A/E (Sca-1) (all antibodies were purchased from BD Biosciences). Finally, lacteal endothelial cells were sorted using a FACS Aria Fusion (BD Biosciences). The isotype-matched control antibody (MAB006; R&D) was used to define the gate threshold of specific antibodies. The lineage-negative gate was obtained by the addition of PE-Cy7 streptavidin-conjugated antibody.

2.14. Western blot analysis

For Western blot analysis, proteins were separated by SDS-PAGE and transferred onto PVDF membranes. These membranes were then incubated with specific antibodies, including *O*-GlcNAc antibody (RL2) (1:1000, MA1-072; Invitrogen, Carlsbad, CA, USA), as well as antibodies against the following molecules: OGT (1:1000, O6264; Sigma-Aldrich); eNOS (1:1000, 32027S; Cell Signaling, Danvers, MA, USA); VEGFR1 (1:1000, AF471; R&D, Minneapolis, MN, USA); VEGFR2 (1:1000, 2479S; Cell Signaling); VEGFR3 (1:1000, AF743; R&D); and β-ACTIN (1:3000, A5316; Sigma-Aldrich). After further washing steps, the membranes were incubated with horseradish peroxidase-linked secondary antibodies, followed by detection using chemiluminescence.

2.15. Total RNA extraction and qRT-PCR analysis

Total RNA was extracted from cells using the RNeasy Kit (Qiagen, Hilden, Germany), and cDNA was synthesized using a reverse-transcription reagent (Takara Bio, Otsu, Japan). The transcript levels were determined by an Applied Biosystems 7500 Real-Time PCR System (PerkinElmer Applied Biosystems, Waltham, MA, USA) using SYBR Green (Bio-Rad Laboratories, Hercules, CA, USA). The analytical data were normalized to *Gapdh* mRNA expression as an internal control. Primer sequences are listed in the Supplemental Table.

2.16. Statistical analysis

Results are expressed as mean ± SEM. The Mann–Whitney *U* test was used to assess the statistical significance of differences between the two groups. For situations where multiple comparisons were necessary, the Kruskal–Wallis rank sum test and a subsequent post hoc Steel–Dwass test were employed to determine the significance. Data were analyzed using commercial software (Prism 9; GraphPad, San Diego, CA, USA), R statistical software version 3.5.2, and EZR [28]. A p value of <0.05 was considered statistically significant.

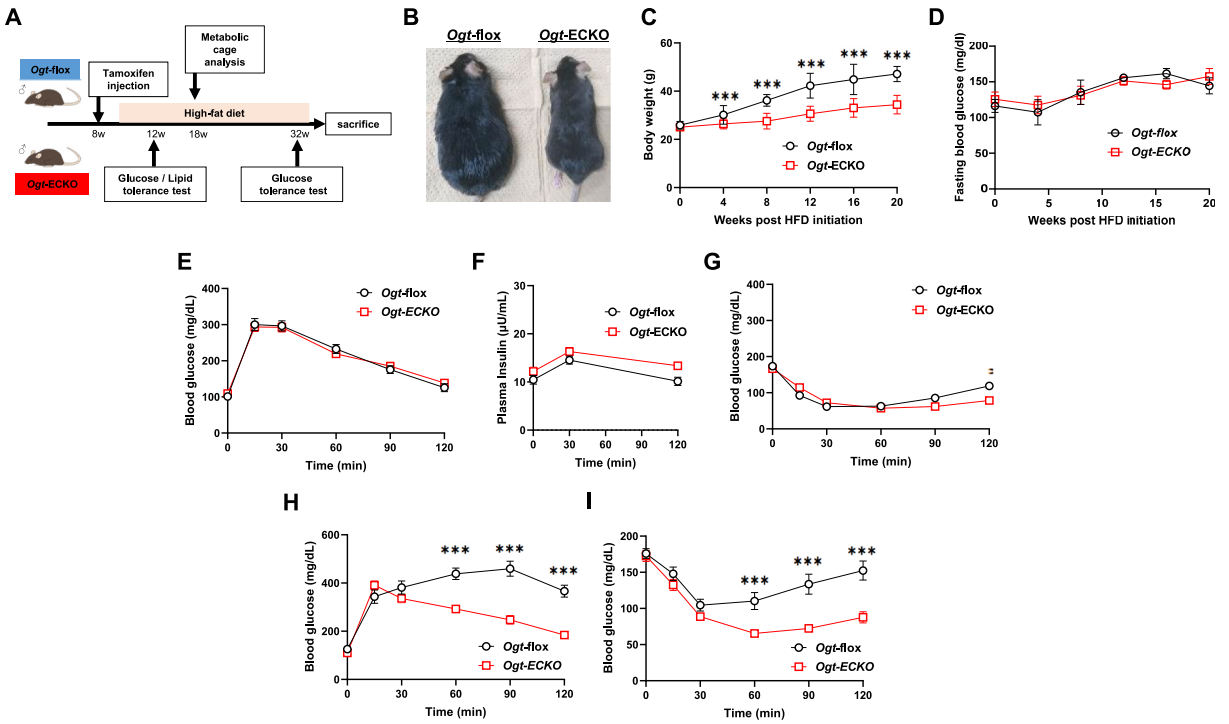

Fig. 2. *Ogt*-ECKO mice did not develop high-fat-diet (HFD)-induced obesity and showed improvement in glucose homeostasis.
A: Overview of the HFD experiment.
B: Representative image of *Ogt*-flox and *Ogt*-ECKO mice fed HFD for 24 weeks (33 weeks of age).
C, D: Body weight (C) and fasting blood glucose levels (D) in *Ogt*-flox and *Ogt*-ECKO mice with HFD (n = 13, each).
E, F: Changes in blood glucose levels (E) and plasma insulin levels (F) during IPGTT after 4 weeks of HFD feeding (13 weeks of age) (n = 13, each).
G: Blood glucose levels during IPITT after 4 weeks of HFD feeding (n = 13, each).
H, I: Blood glucose levels during IPGTT (H) and IPITT (I) in *Ogt*-flox and *Ogt*-ECKO mice after 24 weeks of HFD feeding (33 weeks of age) (n = 13, each).
Data are presented as the mean ± SEM. ***p < 0.001, ns: not statistically significant.

3. Results

3.1. Ogt-ECKO mice exhibited slightly lower body weight gain, but no significant changes in glucose metabolism

To investigate the physiological role of *O*-GlcNAcylation in endothelial cells, we generated mice with endothelial-cell-specific knockout of *Ogt* (*Ogt*-ECKO) by crossbreeding *Ogt*-flox female mice with *VE-CadherinCre-ER*^{T2} male mice (Fig. 1A, Fig. S1). After tamoxifen (TM) injection, the expression of OGT protein in lung vascular endothelial cells was successfully reduced in *Ogt*-ECKO mice compared with that in *Ogt*-flox mice (Fig. 1B).

Four weeks after the TM injection, *Ogt*-ECKO mice had slightly lower body weight than the controls (Fig. 1C). Fasting blood glucose levels did not differ significantly between *Ogt*-ECKO mice and the controls (Fig. 1D). In addition, their plasma glucose and insulin levels during IPGTT were comparable (Fig. 1E and F). Insulin sensitivity examined by IPITT also showed no significant difference between the groups (Fig. 1G). These results suggest that *O*-GlcNAcylation in endothelial cells has a minimal impact on body weight, but no impact on glucose metabolism, under a regular chow diet.

3.2. Weight gain of Ogt-ECKO mice was markedly reduced in the HFD model

Since we observed a slight difference in body weight between *Ogt*-ECKO mice and controls on a regular chow diet, we proceeded to examine the weight difference between the two groups under HFD-induced obesity (Fig. 2A). Interestingly, the weight gain of the *Ogt*-ECKO mice was significantly suppressed compared with that of the controls (Fig. 2B and C). Fasting blood glucose levels remained unchanged over time (Fig. 2D). At 4 weeks after initiating the HFD, no differences were observed in blood glucose levels and plasma insulin levels during IPGTT, indicating comparable glucose tolerance between *Ogt*-ECKO and control mice (Fig. 2E and F). However, blood glucose levels during IPITT were slightly lower in *Ogt*-ECKO mice than in controls (Fig. 2G). These results suggested that the

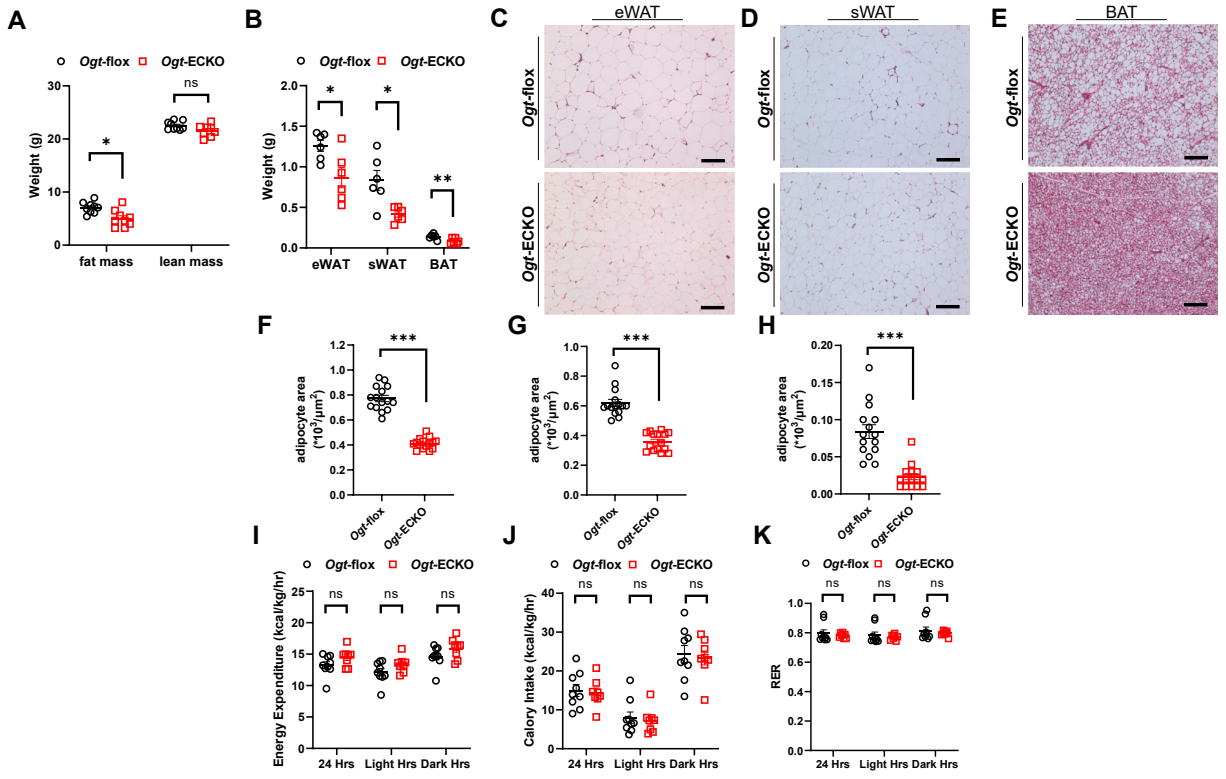

Fig. 3. *Ogt*-ECKO mice had lower adipose tissue weight and smaller lipid droplets in the HFD model.
A, B: Body composition (A) and adipose tissue weight (B) of *Ogt*-flox and *Ogt*-ECKO mice 10 weeks after HFD feeding (19 weeks of age) (n = 8–9).
C–E: Representative images of hematoxylin-eosin staining of eWAT (C), sWAT (D), and BAT (E) of *Ogt*-flox and *Ogt*-ECKO mice 10 weeks after HFD feeding (19 weeks of age). The scale bar represents 20 μm.
F–H: Adipocyte area of eWAT (F), sWAT (G), and BAT (H) in *Ogt*-flox and *Ogt*-ECKO mice 10 weeks after HFD feeding (19 weeks of age) (n = 5 each, 3 fields from each mouse).
I–K: Metabolic study of *Ogt*-flox and *Ogt*-ECKO mice 9 weeks after HFD feeding (18 weeks of age). Energy expenditure (I), caloric intake (J), and respiratory exchange ratio (RER) (K) were monitored (n = 8–9).
Data are presented as the mean ± SEM. *p < 0.05, **p < 0.01, ***p < 0.001, ns: not statistically significant.

glucose tolerance of *Ogt*-ECKO mice was largely unchanged compared with that of *Ogt*-flox mice as early as 4 weeks after starting the HFD.

In contrast, after 24 weeks of HFD feeding, blood glucose levels during IPGTT were significantly improved in *Ogt*-ECKO mice compared with those in *Ogt*-flox mice (Fig. 2H). Additionally, plasma glucose levels during IPITT were significantly decreased in *Ogt*-ECKO mice (Fig. 2I), indicating their improved insulin sensitivity. Taking these findings together, *Ogt*-ECKO mice exhibit significant improvement in HFD-induced obesity and glucose tolerance after long-term HFD feeding.

3.3. Adipose tissue weight was significantly reduced in Ogt-ECKO mice

Next, we conducted a more detailed investigation of the factors contributing to the difference in body weight gain. Body composition analysis showed a significant decrease in fat mass in *Ogt*-ECKO mice, with no difference in lean mass (Fig. 3A). Moreover, a comparison of fat mass among different adipose tissue sites showed that adipose tissue weight of *Ogt*-ECKO mice was significantly reduced in epididymal white adipose tissue (eWAT), subcutaneous white adipose tissue (sWAT), and brown adipose tissue (BAT) (Fig. 3B). Histological analysis also demonstrated significant suppression of adipocyte enlargement in *Ogt*-ECKO mice (Fig. 3C–H). Additionally, *Ogt*-ECKO mice exhibited less liver weight and improved liver function, as indicated by reduced transaminase levels

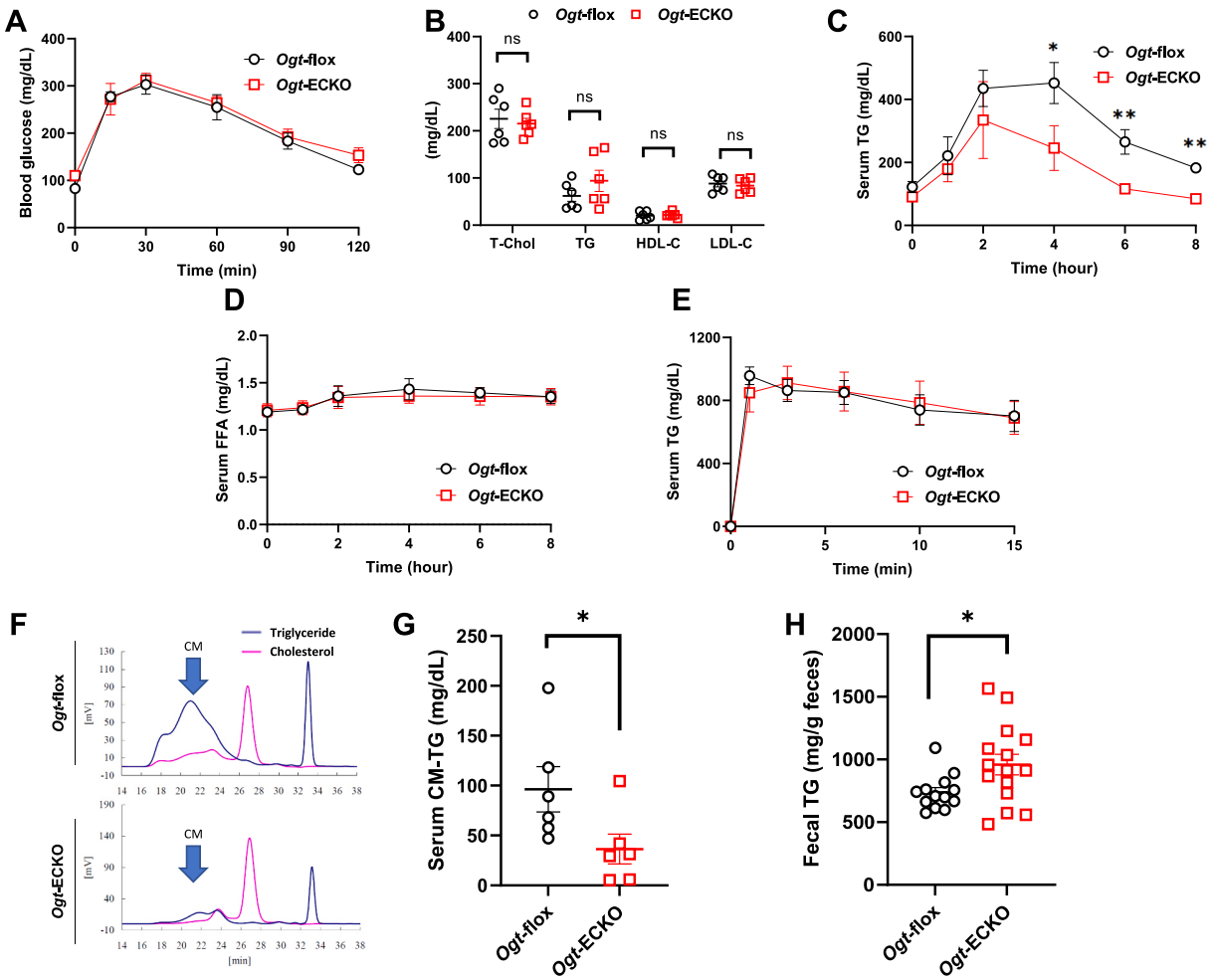

Fig. 4. Oral lipid absorption was significantly reduced in *Ogt*-ECKO mice.
A: Blood glucose levels during OGTT after 4 weeks of HFD feeding (13 weeks of age) (n = 13, each).
B: Results of overnight fasting serum lipid profile of mice after 4 weeks of HFD feeding (13 weeks of age) (n = 6, each).
C, D: Change of serum TG (C) and FFA (D) during oral lipid tolerance test after 4 weeks of HFD feeding (13 weeks of age) (n = 6–7).
E: Change of TG during intravenous lipid tolerance test after 4 weeks of HFD feeding (13 weeks of age) (n = 6–7).
F, G: Results of HPLC analysis with serum at 4 h of OLTT (F) and comparison of CM-TG fraction (G) after 8 weeks of HFD feeding (13 weeks of age) (n = 6, each).
H: Results of fecal TG analysis after 4 weeks of HFD feeding (13 weeks of age) (n = 15–16).
Data are presented as the mean ± SEM. *$p < 0.05$, ns: not statistically significant.

(evaluated using Aspartate aminotransferase (AST) and Alanine aminotransferase (ALT) levels) and hepatic steatosis (Fig. S2B) These results indicated that the significant suppression of body weight gain observed in *Ogt*-ECKO mice under HFD conditions was due not to reductions in lean mass, but rather to reduced fat accumulation. Subsequently, as body weight changes are regulated by caloric intake and energy expenditure, we conducted metabolic cage analysis to determine whether these alterations were the underlying cause of the weight differences. The results showed that O_2 consumption, CO_2 production, basal energy expenditure, activity count, and respiratory exchange ratio (RER) were identical between *Ogt*-flox and *Ogt*-ECKO mice (Fig. 3I–K, Fig. S3).

3.4. Oral lipid absorption was significantly reduced in Ogt-ECKO mice

Next, we hypothesized that nutrient absorption from the intestine might be responsible for the suppression of HFD-induced obesity in *Ogt*-ECKO mice since the mice exhibited resistance to HFD-induced obesity, but no differences in energy expenditure, caloric intake, or respiratory quotient. To investigate this possibility, we first evaluated glucose absorption from the intestine using an OGTT. The results showed no difference in blood glucose level during the OGTT between *Ogt*-flox and *Ogt*-ECKO mice (Fig. 4A). Next, we examined the lipid profiles in fasting and during the OLTT. There were no significant differences in fasting lipid profiles (Fig. 4B); however, serum triglyceride (TG) elevation was significantly suppressed in *Ogt*-ECKO mice during the OLTT, suggesting reduced lipid absorption in these mice (Fig. 4C). Serum FFA levels were comparable between the groups (Fig. 4D). Interestingly, TG levels during the IVLTT were similar between the groups (Fig. 4E). These results support the hypothesis that fat absorption from the intestine is reduced in *Ogt*-ECKO mice. In addition, HPLC analysis of serum at 4 h of the OLTT showed that the increase in TG fraction, particularly the chylomicron (CM)-TG fraction, was significantly suppressed in *Ogt*-ECKO mice (Fig. 4F and G). Simultaneously, TG excretion in stool was significantly increased in *Ogt*-ECKO mice (Fig. 4H). These findings indicate that reduced absorption of lipids from the intestine contributes to the suppression of body weight gain in HFD-fed *Ogt*-ECKO mice.

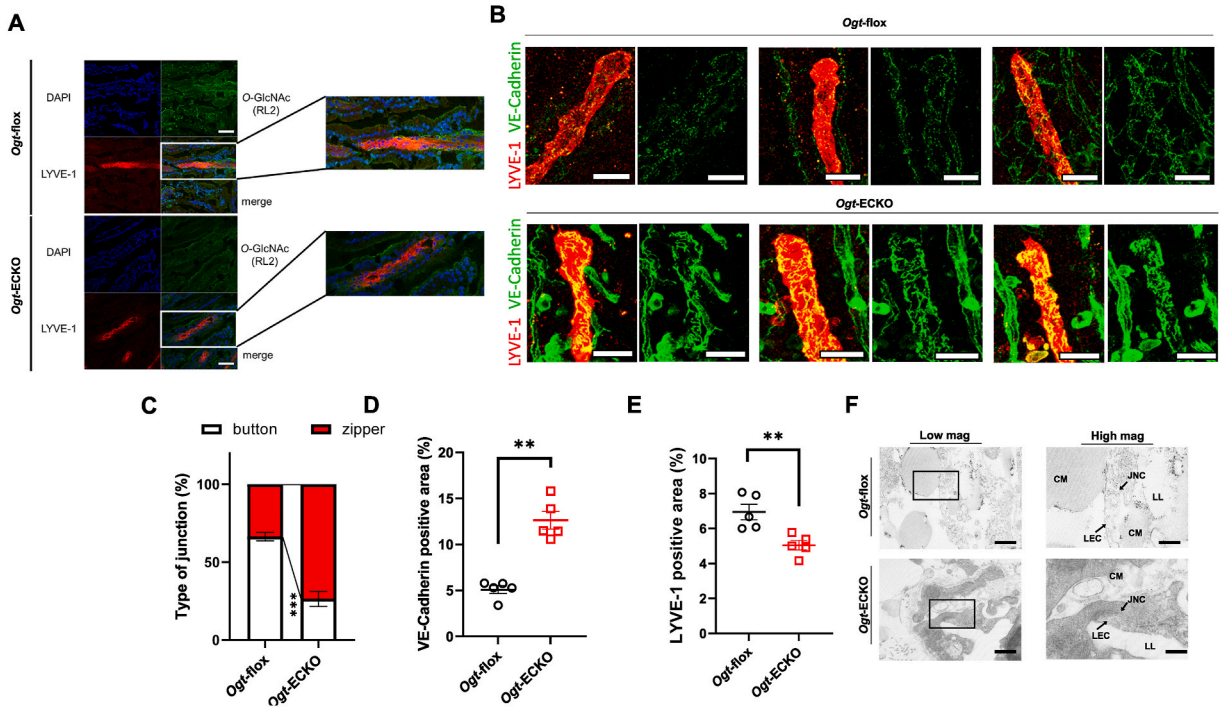

Fig. 5. Reduced lipid absorption from the intestine in *Ogt*-ECKO mice was due to altered intercellular junctions in intestinal lymphatic endothelial cells.

A: Confirmation of *O*-GlcNAc modification expression in LYVE-1-positive cells. The scale bar represents 10 μm.

B–E: Comparative images of intestinal lymphatic endothelial cells, which are positive for both VE-Cadherin and LYVE-1 (B), along with results of percentages of type of junction, button or zipper (C), and percentages of VE-Cadherin- (D) and LYVE-1-positive areas (E). The scale bar represents 10 μm (n = 7, each group).

F: Transmission electron microscopy images comparing the lacteal region of the jejunum in *Ogt*-flox and *Ogt*-ECKO mice after 4 weeks of HFD feeding. LL: lacteal lumen, LEC: lymphatic endothelial cell, CM: chylomicron, JNC: junction. The scale bar represents 500 nm (low magnification) and 200 nm (high magnification).

Data are presented as the mean ± SEM. $^{**}p < 0.01$, $^{***}p < 0.001$.

3.5. Zippering of lacteal lymphatic endothelial cell–cell junctions was responsible for decreased chylomicron absorption

To investigate the underlying mechanism, we performed the morphological evaluation of the intestine. First, we confirmed the loss of *O*-GlcNAcylation in intestinal lymphatic endothelial cells of *Ogt*-ECKO mice through immunofluorescent analysis using the antibody to O-linked *N*-acetylglucosamine and lymphatic endothelial cell-specific marker LYVE-1. (Fig. 5A). VE-cadherin, a component of adherence junction expressed both in lymphatic and vascular endothelial cells, is critical for maintaining junctions between lymphatic endothelial cells. Previous studies have indicated that changes in VE-cadherin adhesion patterns significantly impact lymphatic permeability and the transition between button and zipper junctions [6,27]. Therefore, we examine the morphology of VE-cadherin junctions. Interestingly, the intercellular junctions of lacteal lymphatic endothelial cells in the intestine of *Ogt*-ECKO mice underwent a transformation from "button junctions" into continuous "zipper junctions" (Fig. 5B and C). In addition, the VE-Cadherin-positive area was significantly enlarged, while the LYVE-1-positive region was significantly decreased in the intestinal villi of *Ogt*-ECKO mice (Fig. 5D and E). Transmission electron microscopy further confirmed these changes in the lacteal junctions, and few TG particles were observed in the lacteal lumen of the *Ogt*-ECKO mice (Fig. 5F).

To rule out the possibility that altered lipoprotein lipase (LPL) affects serum TG levels, OLTT and IVLTT were performed under treatment with LPL inhibitors. However, LPL inhibition did not reverse the changes in serum TG (Figs. S4A and B), ruling out the possibility that OGT deficiency affects serum TG concentrations via LPL in vascular endothelial cells. We also examined the release of TG in VLDL from the liver using the VLDL-TG secretion assay, and found that TG in VLDL released from the liver was rather higher in the *Ogt*-ECKO mice (Fig. S4C). These results suggest that the decrease in serum TG in *Ogt*-ECKO mice was not due to changes in LPL or VLDL production from the liver.

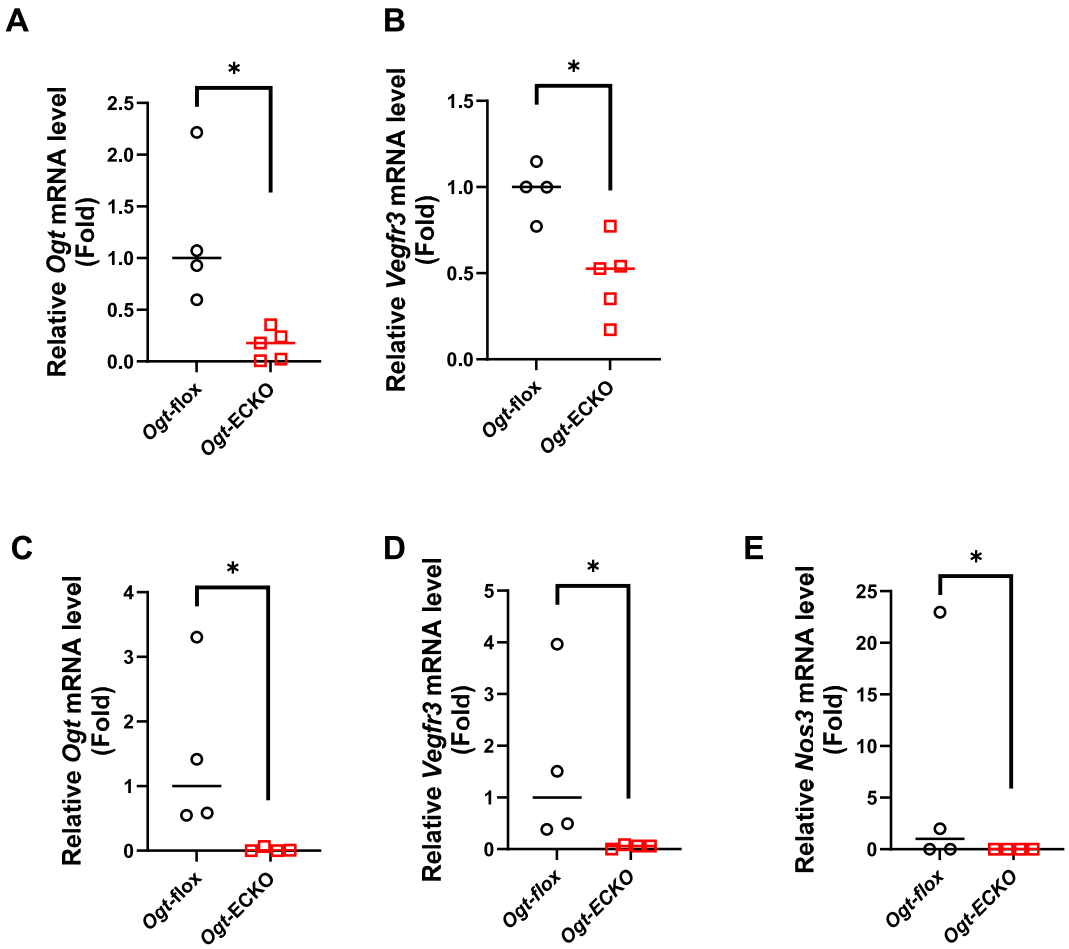

Fig. 6. In *Ogt*-ECKO mice, *Vegfr3* expression was significantly suppressed in both intestinal vascular and lymphatic endothelial cells.
A, B: Quantification of the gene expression of *Ogt* (A) and *Vegfr3* (B) in vascular endothelial cells isolated from mice after 6 weeks of HFD feeding (15 weeks of age) (n = 4–5).
C, D: Quantification of the gene expression of *Ogt* (C), *Vegfr3* (D), and *Nos3* (E) in lacteal endothelial cells isolated from mice after 6 weeks of HFD feeding (15 weeks of age) (n = 4, each).
Data are normalized with *Gapdh* and presented as the mean ± SEM. *$p < 0.05$, ns: not statistically significant.

3.6. Decreased expression of VEGFR3 caused zippering of LECs

Previous reports have shown that ablation of VEGFR1 in vascular endothelium changes the lacteal junction from the button-to the zipper-type configuration [27], which is similar to the findings in *Ogt*-ECKO mice. While isolating sufficient endothelial cells from the intestine for Western blot analysis was challenging, we evaluated the gene expression of *Ogt, Vegfr1, Vegfr2 and Vegfr3 (Flt4)* in vascular and lacteal endothelial cells of mice after 6 weeks of HFD feeding (15-week-old). The expression of the *Ogt* gene was markedly decreased in intestinal vascular endothelial cells isolated from *Ogt*-ECKO mice, and *Vegfr3* gene expression was also significantly reduced (Fig. 6A and B). The protein expression levels of VEGFR1 and VEGFR2 were comparable, but the level of VEGFR3 was lowered in primary cultured vascular endothelial cells from *Ogt*-ECKO mice compared with that in the control (Figs. S5A–C). Similarly, mRNA expression of *Ogt* and *Vegfr3* was significantly lower in lacteal endothelial cells from *Ogt*-ECKO mice than in the control (Fig. 6C and D). Additionally, *Nos3* mRNA expression was significantly lower in *Ogt*-ECKO mice (Fig. 6E).

As VEGFR3 has been reported to be involved in lymphatic maintenance in the intestine and TG absorption [22], we hypothesized that triglyceride absorption is reduced in *Ogt*-ECKO mice through the VEGFC–VEGFR3 pathway. VEGFC–VEGFR3 signaling is known to be important in the production of nitric oxide (NO), which influences the permeability of lymphatic vessels [29]. Given the decreased *Nos3* expression in *Ogt*-ECKO mice (Fig. 6E), we measured serum NO concentrations. The results showed significantly lower levels of NO in *Ogt*-ECKO mice than in *Ogt*-flox mice (Fig. 7A). Therefore, we hypothesized that restoring the decrease in serum NO levels may improve lipid absorption from the intestine. To investigate this, we performed an OLTT with DETA-NONOate, a NO donor (Fig. S6). As expected, *Ogt*-ECKO mice receiving NO donor gained more body weight (Fig. 7B). In addition, the decreased serum TG level during OLTT in *Ogt*-ECKO mice returned to levels similar to those of *Ogt*-flox mice, the untreated control group (Fig. 7C). TEM analysis also showed intestinal lacteal endothelial cell-to-cell junctions, confirming the opening of zipper junctions and migration of TG into the lacteal vessels in *Ogt*-ECKO mice with NO donor (Fig. 7D).

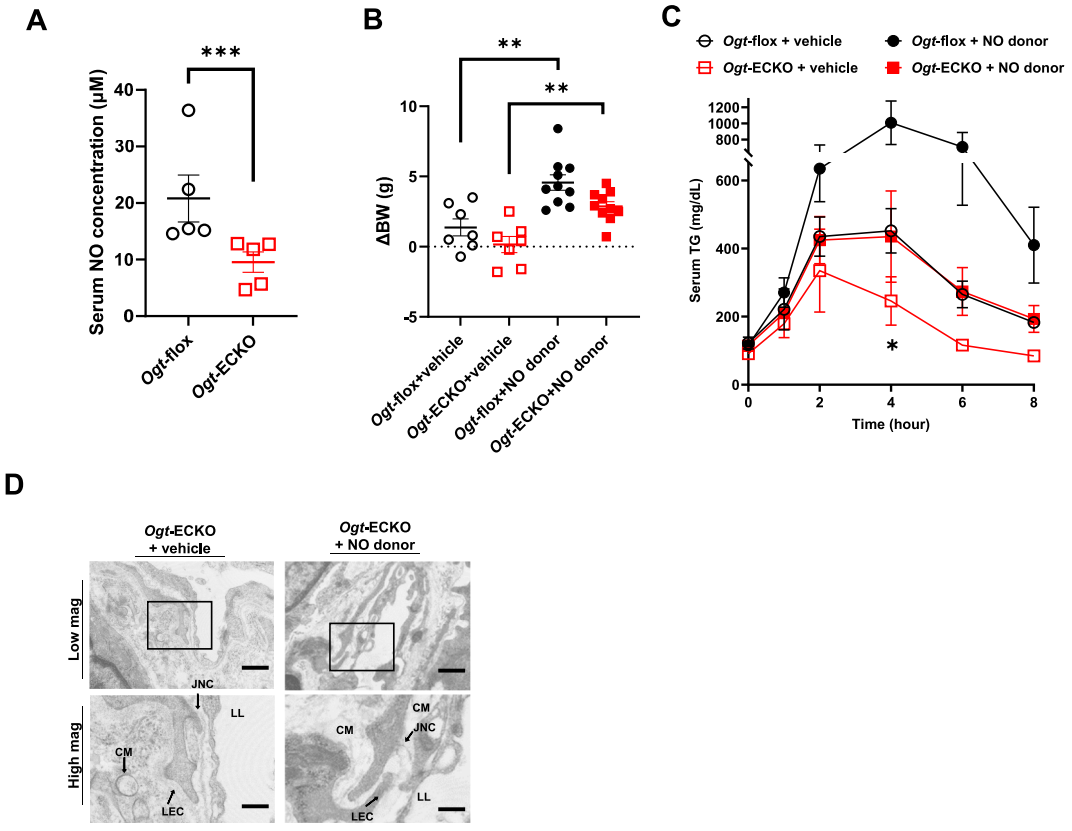

Fig. 7. In *Ogt*-ECKO mice, lacteal junction zippering inhibited lipid absorption from the intestine, which was recovered by NO donor supplementation.

A: Serum NO concentration of *Ogt*-flox and *Ogt*-ECKO mice after 4 weeks of HFD feeding (13 weeks of age).

B: Weight change between before and after NO donor administration (n = 7–10, each).

C: OLTT results of *Ogt*-flox, *Ogt*-ECKO, NO donor-treated *Ogt*-flox, and *Ogt*-ECKO mice after 4 weeks of HFD feeding (n = 7–10, each).

D: Representative transmission electron microscopy image of the lacteal region in the jejunum from *Ogt*-ECKO mice with DETA NONOate after 4 weeks of HFD feeding. LL: lacteal lumen, LEC: lymphatic endothelial cell, CM: chylomicron, JNC: junction.

The scale bar represents 500 nm (low magnification) and 200 nm (high magnification).

Data are presented as the mean ± SEM. *p < 0.05, **p < 0.01, ***p < 0.001.

In summary, our study revealed that *Ogt*-ECKO mice exhibited reduced intestinal fat absorption during HFD loading, likely due to reduced VEGFC–VEGFR3 signaling-mediated NO production. This suggests that *O*-GlcNAcylation in endothelial cells plays an important role in intestinal fat absorption.

4. Discussion

The current study aimed to determine the role of *O*-GlcNAcylation in endothelial cells and made three important findings. First, we found that *Ogt*-ECKO mice had less diet-induced weight gain than *Ogt*-flox control mice and were resistant to HFD-induced obesity. Second, we discovered that *O*-GlcNAcylation in endothelial cells is responsible for fat absorption from the intestine and identified alterations of intercellular junctions of intestinal lymphatic endothelial cells that affect fat absorption. Third, supplementation of a NO donor recovered fat absorption in *Ogt*-ECKO mice.

We observed that the loss of *O*-GlcNAcylation appeared to result in less body weight gain under an HFD than in *Ogt*-flox control mice (Fig. 2C). Generally, body weight is regulated by the balance between caloric intake and energy expenditure. Previous reports have shown that the loss of *O*-GlcNAcylation in paraventricular nucleus (PVN) neurons leads to weight gain due to overeating [30], while the loss of *O*-GlcNAcylation in adipose tissue results in less fat accumulation due to dysregulation of perilipin and increased lipolysis [14,30]. Furthermore, acquired loss of *O*-GlcNAcylation in pancreatic β-cells induced excessive insulin secretion, leading to weight gain despite normal caloric intake [14,31]. These findings suggest the significant role of *O*-GlcNAcylation in sensing nutritional status in various organs [32]. We found no significant differences in energy expenditure and caloric intake between *Ogt*-ECKO mice and controls (Fig. 3A and B). Therefore, we hypothesized that the difference in body weight gain between *Ogt*-ECKO and *Ogt*-flox control mice may be attributable to differences in macronutrient absorption.

To confirm our hypothesis that macronutrient absorption from the intestine is impaired in *Ogt*-ECKO mice, we performed OGTT and OLTT. Interestingly, the OGTT showed no significant difference in *Ogt*-ECKO mice and controls (Fig. 4A), while the OLTT indicated suppression of the increase in triglycerides after oil loading (Fig. 4C). Additionally, IVLTT revealed no difference in triglyceride levels between the two groups (Fig. 4E), suggesting that lipid metabolism after absorption was intact. Fecal triglyceride levels were higher in *Ogt*-ECKO mice than in controls (Fig. 4H), indicating that the reduced weight gain observed in *Ogt*-ECKO mice was due to impaired fat absorption from the intestine. Previously, we found that mice with whole-body OGT deficiency showed weight loss and a lethal phenotype [14]. Moreover, mice with OGT knockout in intestinal epithelial cells exhibited lower body weight and impaired glucose absorption due to reduced sodium-glucose cotransporter-1 expression [32]. These findings strongly suggest that *O*-GlcNAcylation plays an important role in nutritional absorption.

To explore the mechanism underlying fat malabsorption in the intestine of *Ogt*-ECKO mice, we focused on the structure of lymphatic endothelial cells. We found increased zippering of intercellular junctions in intestinal lacteal endothelial cells of *Ogt*-ECKO mice (Fig. 5A and B) and TG particles were absent from the lymphatic vessels (Fig. 5E). Dietary fat is digested by bile and pancreatic lipase and then absorbed by intestinal epithelial cells. Subsequently, chylomicrons are synthesized in the intestinal epithelial cells and transported into the lymphatics through the open button-like junction [33]. A “button junction” is a structure where adjacent lymphatic endothelial cells loosely adhere to each other. Due to the presence of numerous gaps, lipid drainage occurs via pressure gradients. In contrast, a “zipper junction” involves tight adhesion between lymphatic endothelial cells. With fewer gaps, drainage is not sufficiently facilitated by pressure gradients alone. As a result, the transition from “button” to “zipper” leads to decreased absorption of lipids and other substances [34]. A recent report has shown that zippering of the open button-like junctions in lacteal endothelial cells decreases fat absorption in the small intestine. VEGFR1 and VEGFR2 are involved in the zippering of lacteal junctions, and acquired VEGFR1 deficiency causes zippering of lymphatic endothelial cells through the activation of VEGFR2 [34]. In our study, the expression of VEGFR1 and VEGFR2 proteins did not significantly differ between *Ogt*-ECKO and control mice (Figs. S5A and B). However, VEGFR3 expression was significantly decreased in vascular and lymphatic endothelial cells of *Ogt*-ECKO mice (Fig. 6B–D, S5C). The underlying mechanisms are unclear, but a recent report showed that Forkhead box P1 (FOXP1), a transcription factor that regrates multiple differentiation pathways during development, negatively regulates VEGFR3 expression through the suppression of Tumor necrosis factor superfamily 15 (TNFSF15) which belongs to the tumor necrosis factor ligand family and serve as an angiogenesis inhibitor [35,36]. TNFSF15 has been reported to upregulate VEGFR3 expression in lymphatic endothelial cells [37]. Since FOXP1 is a known target protein for *O*-GlcNAcylation [38], it is possible that FOXP1 is involved in the decreased expression of VEGFR3 in *Ogt*-ECKO mice.

We then hypothesized that supplementation of NO donor improve fat absorption from the intestine, as VEGFR3 activation increases NO secretion from endothelial cells [38]. We found that NO donor supplementation rescued triglyceride absorption in *Ogt*-ECKO mice, as evidenced by OLTT results that were comparable to those of control mice (Fig. 7C). Additionally, electron microscopy revealed the migration of lipids into the lymphatic vessels, accompanied by open zippering of the lacteal junctions (Fig. 7D). These findings suggest that *O*-GlcNAcylation in endothelial cells plays a crucial role in fat absorption in the intestine through the regulation of VEGFR3-NO pathway.

However, the extent to which NO production in lymphatic endothelial cells affects blood NO concentration remains unclear. In addition, more than 1000 proteins have been reported to be *O*-GlcNAc modified, which may have a variety of effects on cellular function [39]. It is possible that pathways other than the NO pathway are involved in the fat absorption defects observed in this study, and further investigation is needed.

Regarding the impact of endothelial *O*-GlcNAcylation on glucose metabolism, *Ogt*-ECKO mice on an HFD for 24 weeks exhibited improved insulin sensitivity and glucose tolerance compared with controls (Fig. 2H and I). Since neither insulin sensitivity nor glucose tolerance was improved in the normal-diet group, and glucose tolerance was not improved after 4 weeks of an HFD, the difference in glucose tolerance in the group consuming an HFD for 24 weeks was not directly due to a loss of *O*-GlcNAcylation in endothelial cells,

but likely due to differences in body weight gain.

In this study, we discovered that the loss of *O*-GlcNAcylation in endothelial cells ameliorated HFD-induced obesity by suppressing lipid absorption in the intestine. Although obesity is increasing worldwide and has become a global health problem, effective weight loss therapies are limited. In addition to the present results, inducible knockout of OGT specifically in the intestinal epithelium has been reported to regulate glucose absorption and induce body weight reduction [15]. *O*-GlcNAcylation is a potential therapeutic target for improving obesity using an intestine-restricted agent.

In conclusion, *O*-GlcNAcylation in endothelial cells plays a crucial role in fat absorption. Although further studies are needed to clarify the direct targets of *O*-GlcNAcylation, this study provides new insights into the biology of endothelial cells and may be useful in the treatment of obesity.

Ethics statement

All animal handling and experimentation were conducted in accordance with the Research Center for Animal Life Science guidelines at Shiga University of Medical Science (approval numbers 28–32, 31–45, and 3–14) or Yale University. All experimental protocols were approved by the Gene Recombination Experiment Safety Committee and Research Center for Animal Life Science at Shiga University of Medical Science or Yale University Institutional Animal Care and Use Committee.

Data availability

All data and materials are available from the corresponding authors upon reasonable request.

Funding

This study was supported by Grants-in-Aid for Scientific Research (KAKENHI) from the Japan Society for the Promotion of Science, Japan (HM 18H02862, SU 19K08998). This study was also supported by the United States Public Health Service (P30 DK045735, UC2DK13491, R01DK133143 to GIS). This study was supported in part by the Japan Foundation for Applied Enzymology, Japan (to NO). This study was also supported by research promotion grants from Nipro, Bayer Yakuhin, Boehringer-Ingelheim, Kyowa Hakko Kirin, Kowa Pharmaceuticals, Sumitomo Dainippon Pharma Co., Ltd., Daiichi-Sankyo, Takeda Pharmaceutical Company Limited, Novo Nordisk, Mitsubishi Tanabe, Sanwa Kagaku Kenkyusho, MSD, and Mochida Pharmaceutical Co., Ltd.

CRediT authorship contribution statement

Seiichiro Ohgaku: Writing – original draft, Methodology, Investigation, Formal analysis, Data curation, Conceptualization. **Shogo Ida:** Writing – review & editing, Writing – original draft, Visualization, Supervision, Project administration, Investigation, Funding acquisition, Formal analysis, Data curation, Conceptualization. **Natsuko Ohashi:** Writing – review & editing, Writing – original draft, Visualization, Supervision, Methodology, Investigation, Funding acquisition, Data curation, Conceptualization. **Katsutaro Morino:** Writing – review & editing, Writing – original draft, Supervision, Conceptualization. **Atsushi Ishikado:** Writing – review & editing, Investigation. **Tsuyoshi Yanagimachi:** Writing – review & editing, Supervision. **Koichiro Murata:** Writing – review & editing, Supervision. **Daisuke Sato:** Writing – review & editing, Supervision. **Satoshi Ugi:** Writing – review & editing, Supervision. **Ali Nasiri:** Writing – review & editing, Methodology, Investigation, Data curation. **Gerald I. Shulman:** Writing – review & editing, Supervision. **Hiroshi Maegawa:** Writing – review & editing, Supervision. **Shinji Kume:** Writing – review & editing, Supervision. **Yukihiro Fujita:** Writing – review & editing, Writing – original draft, Supervision, Conceptualization.

Declaration of competing interest

The authors declare the following financial interests/personal relationships which may be considered as potential competing interests:Hiroshi Maegawa reports financial support was provided by Japan Society for the Promotion of Science. Satoshi Ugi reports financial support was provided by Japan Society for the Promotion of Science. Gerald I. Shulman reports financial support was provided by US Public Health Services. Natsuko Ohashi reports financial support was provided by Japan Foundation for Applied Enzymology. Shinji Kume reports financial support was provided by Nipro Corporation. Shinji Kume reports financial support was provided by Bayer Yakuhin Kabushiki Kaisha. Shinji Kume reports financial support was provided by Boehringer Ingelheim Ltd. Shinji Kume reports financial support was provided by Kyowa Hakko Kirin Pharma Inc. Shinji Kume reports financial support was provided by Kowa Pharmaceutical Co Ltd. Shinji Kume reports financial support was provided by Sumitomo Pharma Co Ltd. Shinji Kume reports financial support was provided by Daiichi Sankyo Inc. Shinji Kume reports financial support was provided by Takeda Pharmaceutical Company Limited. Shinji Kume reports financial support was provided by Novo Nordisk Inc. Shinji Kume reports financial support was provided by Mitsubishi Tanabe Pharma Corporation. Shinji Kume reports financial support was provided by Sanwa Kagaku Kenkyusho Co Ltd. Shinji Kume reports financial support was provided by MSD Pharmaceutical. Shinji Kume reports financial support was provided by Mochida Pharmaceutical Co Ltd. If there are other authors, they declare that they have no known competing financial interests or personal relationships that could have appeared to influence the work reported in this paper.

Acknowledgments

We are indebted to Keiko Kosaka, Takefumi Yamamoto (Shiga University of Medical Science), and staff at the Central Research Laboratory of Shiga University of Medical Science for their expert technical assistance in this study. We are also grateful to Dr. Yoshiaki Kubota (Keio University School of Medicine) and Dr. Masatsugu Ema (Shiga University of Medical Science) for providing the *VE-Cadherin* Cre ER^{T2} mice. Thanks also go to Dr. Yusuke Ichiyama for support with the procedures and advice on experimental techniques. Finally, we thank Edanz (https://jp.edanz.com/ac) for editing a draft of this manuscript.

Appendix A. Supplementary data

Supplementary data to this article can be found online at https://doi.org/10.1016/j.heliyon.2024.e34490.

References

[1] M. Potente, T. Mäkinen, Vascular heterogeneity and specialization in development and disease, Nat. Rev. Mol. Cell Biol. 18 (2017) 477–494, https://doi.org/10.1038/nrm.2017.36.
[2] T. Tammela, K. Alitalo, Lymphangiogenesis: molecular mechanisms and future promise, Cell 140 (2010) 460–476, https://doi.org/10.1016/j.cell.2010.01.045.
[3] B.G. Coon, N. Baeyens, J. Han, M. Budatha, T.D. Ross, J.S. Fang, S. Yun, J.-L. Thomas, M.A. Schwartz, Intramembrane binding of VE-cadherin to VEGFR2 and VEGFR3 assembles the endothelial mechanosensory complex, J. Cell Biol. 208 (2015) 975–986, https://doi.org/10.1083/jcb.201408103.
[4] R. Hägerling, E. Hoppe, C. Dierkes, M. Stehling, T. Makinen, S. Butz, D. Vestweber, F. Kiefer, Distinct roles of VE-cadherin for development and maintenance of specific lymph vessel beds, EMBO J. 37 (2018), https://doi.org/10.15252/embj.201798271.
[5] Y. Yang, B. Cha, Z.Y. Motawe, R.S. Srinivasan, J.P. Scallan, VE-cadherin is required for lymphatic Valve formation and maintenance, Cell Rep. 28 (2019) 2397–2412.e4, https://doi.org/10.1016/j.celrep.2019.07.072.
[6] V. Cifarelli, S. Appak-Baskoy, V.S. Peche, A. Kluzak, T. Shew, R. Narendran, K.M. Pietka, M. Cella, C.W. Walls, R. Czepielewski, S. Ivanov, G.J. Randolph, H. G. Augustin, N.A. Abumrad, Visceral obesity and insulin resistance associate with CD36 deletion in lymphatic endothelial cells, Nat. Commun. 12 (2021) 3350, https://doi.org/10.1038/s41467-021-23808-3.
[7] F. Zhang, G. Zarkada, J. Han, J. Li, A. Dubrac, R. Ola, G. Genet, K. Boyé, P. Michon, S.E. Künzel, J.P. Camporez, A.K. Singh, G.-H. Fong, M. Simons, P. Tso, C. Fernández-Hernando, G.I. Shulman, W.C. Sessa, A. Eichmann, Lacteal junction zippering protects against diet-induced obesity, Science 361 (2018) 599–603, https://doi.org/10.1126/science.aap9331.
[8] M.R. Bond, J.A. Hanover, O-GlcNAc cycling: a link between metabolism and chronic disease, Annu. Rev. Nutr. 33 (2013) 205–229, https://doi.org/10.1146/annurev-nutr-071812-161240.
[9] K. Vaidyanathan, S. Durning, L. Wells, Functional O-GlcNAc modifications: implications in molecular regulation and pathophysiology, Crit. Rev. Biochem. Mol. Biol. 49 (2014) 140–163, https://doi.org/10.3109/10409238.2014.884535.
[10] X. Yang, K. Qian, Protein O-GlcNAcylation: emerging mechanisms and functions, Nat. Rev. Mol. Cell Biol. 18 (2017) 452–465, https://doi.org/10.1038/nrm.2017.22.
[11] H.-B. Ruan, J.P. Singh, M.-D. Li, J. Wu, X. Yang, Cracking the O-GlcNAc code in metabolism, Trends endocrinol, Metab. 24 (2013) 301–309, https://doi.org/10.1016/j.tem.2013.02.002.
[12] J. Janetzko, S. Walker, The making of a sweet modification: structure and function of O-GlcNAc transferase, J. Biol. Chem. 289 (2014) 34424–34432, https://doi.org/10.1074/jbc.R114.604405.
[13] M. Brownlee, Biochemistry and molecular cell biology of diabetic complications, Nature 414 (2001) 813–820, https://doi.org/10.1038/414813a.
[14] S. Ida, K. Morino, O. Sekine, N. Ohashi, S. Kume, T. Chano, K. Iwasaki, N. Harada, N. Inagaki, S. Ugi, H. Maegawa, Diverse metabolic effects of O-GlcNAcylation in the pancreas but limited effects in insulin-sensitive organs in mice, Diabetologia 60 (2017) 1761–1769, https://doi.org/10.1007/s00125-017-4327-y.
[15] K. Nishimura, Y. Fujita, S. Ida, T. Yanagimachi, N. Ohashi, K. Nishi, A. Nishida, Y. Iwasaki, K. Morino, S. Ugi, E. Nishi, A. Andoh, H. Maegawa, Glycaemia and body weight are regulated by sodium-glucose cotransporter 1 (SGLT1) expression via O-GlcNAcylation in the intestine, Mol. Metabol. 59 (2022) 101458, https://doi.org/10.1016/j.molmet.2022.101458.
[16] M. Zhao, X. Xiong, K. Ren, B. Xu, M. Cheng, C. Sahu, K. Wu, Y. Nie, Z. Huang, R.S. Blumberg, X. Han, H.-B. Ruan, Deficiency in intestinal epithelial O-GlcNAcylation predisposes to gut inflammation, EMBO Mol. Med. 10 (2018), https://doi.org/10.15252/emmm.201708736.
[17] Y. Yang, M. Fu, M.-D. Li, K. Zhang, B. Zhang, S. Wang, Y. Liu, W. Ni, Q. Ong, J. Mi, X. Yang, O-GlcNAc transferase inhibits visceral fat lipolysis and promotes diet-induced obesity, Nat. Commun. 11 (2020) 181, https://doi.org/10.1038/s41467-019-13914-8.
[18] A. Nakamoto, N. Ohashi, L. Sugawara, K. Morino, S. Ida, R.J. Perry, I. Sakuma, T. Yanagimachi, Y. Fujita, S. Ugi, S. Kume, G.I. Shulman, H. Maegawa, O-linked N-acetylglucosamine modification is essential for physiological adipose expansion induced by high-fat feeding, Am. J. Physiol. Endocrinol. Metab. 325 (2023) E46–E61, https://doi.org/10.1152/ajpendo.00263.2022.
[19] C.-L. Dai, J.-H. Gu, F. Liu, K. Iqbal, C.-X. Gong, Neuronal O-GlcNAc transferase regulates appetite, body weight, and peripheral insulin resistance, Neurobiol. Aging 70 (2018) 40–50, https://doi.org/10.1016/j.neurobiolaging.2018.05.036.
[20] K. Zhang, R. Yin, X. Yang, O-GlcNAc: a bittersweet switch in liver, Front. Endocrinol. 5 (2014) 221, https://doi.org/10.3389/fendo.2014.00221.
[21] K. Sakai, J.i. Miyazaki, A transgenic mouse line that retains Cre recombinase activity in mature oocytes irrespective of the cre transgene transmission, Biochem. Biophys. Res. Commun. 237 (1997) 318–324, https://doi.org/10.1006/bbrc.1997.7111.
[22] H. Nurmi, P. Saharinen, G. Zarkada, W. Zheng, M.R. Robciuc, K. Alitalo, VEGF-C is required for intestinal lymphatic vessel maintenance and lipid absorption, EMBO Mol. Med. 7 (2015) 1418–1425, https://doi.org/10.15252/emmm.201505731.
[23] W.J.D. E G Bligh, A rapid method of total lipid extraction and purification, Can. J. Biochem. Physiol. . (n.d.). https://doi.org/10.1139/o59-099.
[24] M.E. Kotas, M.J. Jurczak, C. Annicelli, M.P. Gillum, G.W. Cline, G.I. Shulman, R. Medzhitov, Role of caspase-1 in regulation of triglyceride metabolism, Proc. Natl. Acad. Sci. U.S.A. 110 (2013) 4810–4815, https://doi.org/10.1073/pnas.1301996110.
[25] E.P. Newberry, Y. Xie, S. Kennedy, X. Han, K.K. Buhman, J. Luo, R.W. Gross, N.O. Davidson, Decreased hepatic triglyceride accumulation and altered fatty acid uptake in mice with deletion of the liver fatty acid-binding protein gene, J. Biol. Chem. 278 (2003) 51664–51672, https://doi.org/10.1074/jbc.M309377200.
[26] A. Salas, M. Gironella, A. Salas, A. Soriano, M. Sans, J. Iovanna, J.M. Piqué, J. Panés, Nitric oxide supplementation ameliorates dextran sulfate sodium-induced colitis in mice, Lab. Invest. 82 (2002) 597–607, https://doi.org/10.1038/labinvest.3780454.
[27] M. Katagi, T. Terashima, N. Ohashi, Y. Nakae, A. Yamada, T. Nakagawa, I. Miyazawa, H. Maegawa, J. Okano, Y. Suzuki, K. Fujino, Y. Eguchi, H. Kojima, Malfunctioning CD106-positive, short-term hematopoietic stem cells trigger diabetic neuropathy in mice by cell fusion, Commun. Biol. 4 (2021) 575, https://doi.org/10.1038/s42003-021-02082-5.
[28] Y. Kanda, Investigation of the freely available easy-to-use software "EZR" for medical statistics, Bone Marrow Transplant. 48 (2013) 452–458, https://doi.org/10.1038/bmt.2012.244.

[29] T. Shew, N.E. Wolins, V. Cifarelli, VEGFR-3 signaling regulates triglyceride retention and absorption in the intestine, Front. Physiol. 9 (2018) 1783, https://doi.org/10.3389/fphys.2018.01783.
[30] O. Lagerlöf, J.E. Slocomb, I. Hong, Y. Aponte, S. Blackshaw, G.W. Hart, R.L. Huganir, The nutrient sensor OGT in PVN neurons regulates feeding, Science 351 (2016) 1293–1296, https://doi.org/10.1126/science.aad5494.
[31] R. Mohan, S. Jo, E. Da Sol Chung, E. Oribamise, A. Lockridge, J.E. Abrahante-Lloréns, H.-B. Ruan, X.-Y. Yang, E.U. Alejandro, Pancreatic β-cell O-GlcNAc transferase overexpression increases susceptibility to metabolic stressors in female mice, Cells 10 (2021), https://doi.org/10.3390/cells10102801.
[32] K. Morino, H. Maegawa, Role of O-linked N-acetylglucosamine in the homeostasis of metabolic organs, and its potential links with diabetes and its complications, J. Diabetes Investig. 12 (2021) 130–136, https://doi.org/10.1111/jdi.13359.
[33] P.R. Norden, T. Kume, Molecular mechanisms controlling lymphatic endothelial junction integrity, Front. Cell Dev. Biol. 8 (2020) 627647, https://doi.org/10.3389/fcell.2020.627647.
[34] F. Zhang, G. Zarkada, S. Yi, A. Eichmann, Lymphatic endothelial cell junctions: molecular regulation in physiology and diseases, Front. Physiol. 11 (2020) 509, https://doi.org/10.3389/fphys.2020.00509.
[35] G.-L. Yang, L.-Y. Li, Counterbalance: modulation of VEGF/VEGFR activities by TNFSF15, Signal Transduct. Targeted Ther. 3 (2018) 21, https://doi.org/10.1038/s41392-018-0023-8.
[36] H. Li, P. Liu, S. Xu, Y. Li, J.D. Dekker, B. Li, Y. Fan, Z. Zhang, Y. Hong, G. Yang, T. Tang, Y. Ren, H.O. Tucker, Z. Yao, X. Guo, FOXP1 controls mesenchymal stem cell commitment and senescence during skeletal aging, J. Clin. Invest. 127 (2017) 1241–1253, https://doi.org/10.1172/JCI89511.
[37] T.-T. Qin, G.-C. Xu, J.-W. Qi, G.-L. Yang, K. Zhang, H.-L. Liu, L.-X. Xu, R. Xiang, G. Xiao, H. Cao, Y. Wei, Q.-Z. Zhang, L.-Y. Li, Tumour necrosis factor superfamily member 15 (Tnfsf15) facilitates lymphangiogenesis via up-regulation of Vegfr3 gene expression in lymphatic endothelial cells, J. Pathol. 237 (2015) 307–318, https://doi.org/10.1002/path.4577.
[38] J.F. Alfaro, C.-X. Gong, M.E. Monroe, J.T. Aldrich, T.R.W. Clauss, S.O. Purvine, Z. Wang, D.G. Camp, J. Shabanowitz, P. Stanley, G.W. Hart, D.F. Hunt, F. Yang, R.D. Smith, Tandem mass spectrometry identifies many mouse brain *O*-GlcNAcylated proteins including EGF domain-specific *O*-GlcNAc transferase targets, Proc. Natl. Acad. Sci. U.S.A. 109 (2012) 7280–7285, https://doi.org/10.1073/pnas.1200425109.
[39] A.K. Nagel, L.E. Ball, O-GlcNAc transferase and O-GlcNAcase: achieving target substrate specificity, Amino Acids 46 (2014) 2305–2316, https://doi.org/10.1007/s00726-014-1827-7.